VCST Internal Memo

Title: Absolute Spectral Response Derived from T-SIRCUS Polarization Measurements for JPSS-1 VIIRS
Memo Number: 2016_008
Revision: 01
Date: June 1, 2016
Author: Jeff McIntire
To: Xiaoxiong Xiong and James Butler
Cc: Hassan Oudrari, Kwo-Fu (Vincent) Chiang, Jon Fulbright and Aisheng Wu

---

References

[1] 'VNIR Polarization Sensitivity vs Wavelength using the T-SIRCUS,' Raytheon.
[2] "Facility for spectral irradiance and radiance responsivity calibrations using uniform sources," S. W. Brown, G. P. Eppeldauer, and K. R. Lykke, Appl. Opt. 45(32), 8218–8237 (2006).
[3] "Analysis of JPSS J1 VIIRS Polarization Sensitivity Using the NIST T-SIRCUS," Jeff McIntire, Jim Young, Dave Moyer, Gene Waluschka, Hassan Oudrari, and Jack Xiong. Proc. SPIE. 9607, 960713 (2015).
[4] "VIIRS/J1 Polarization Narrative," Eugene Waluschka, Joel McCorkel, Jeff McIntire, Dave Moyer, Brendan McAndrew, Steve Brown, Keith Lykke, Jim Young, Eric Fest, Jim Butler, Tung Wang, Eslim Monroy, Kevin Turpie, Gerhard Meister, and Kurt Thome, Proc. SPIE. 9607, 960712 (2015).
[5] VCST_TECH_MEMO_2015_016, 'Polarization Sensitivity Measurements for the JPSS J1 VIIRS VisNIR Bands Using the NIST T-SIRCUS,' Jeff McIntire, September 1, 2015.
[6] "Comparison of two methodologies for calibrating satellite in the visible and near-infrared," Robert Barnes, Steven Brown, Keith Lykke, Bruce Guenther, James Butler, Thomas Schwarting, Kevin Turpie, David Moyer, Frank DeLuccia, and Christopher Moeller, Appl. Opt. 54(35), 10376 (2015).
[7] VCST_TECH_REPORT_15_004, 'Absolute Spectral Response Derived from T-SIRCUS Polarization Testing,' Jeff McIntire, February 19, 2015.
[8] "Measured Polarized Spectral Responsivity of JPSS J1 VIIRS Using the NIST T-SIRCUS," Jeff McIntire, Jim Young, Dave Moyer, Gene Waluschka, and Jack Xiong, Proc. SPIE. 9607, 96072D (2015).
[9] VCST_TECH_MEMO_2015_002, 'Assessment of FP-11' Polarization Sensitivity for the JPSS J1 VIIRS VisNIR Bands and Comparison to FP-11 Measurements,' Jeff McIntire, February 12, 2015.
[10] VCST_TECH_REPORT_15_003, 'Preliminary Analysis of J1 SIRCUS RSR Testing,' Tom Schwarting and Jeff McIntire, January 8, 2015.
[11] VCST_TECH_MEMO_2015_017, 'Polarization Sensitivity Measurements for the JPSS J1 VIIRS DNB Using the NIST T-SIRCUS,' Jeff McIntire, September 1, 2015.
[12] "Preliminary assessment of JPSS-1 VIIRS pre-launch radiometric performance," Hassan Oudrari, Jeff McIntire, Jack Xiong, Jim Butler, Boryana Efremova, Jack Ji, Shihyan Lee, and Tom Schwarting, Proc. SPIE. 9607, 960710 (2015).

1. Introduction

JPSS J1 VIIRS sensor polarization sensitivity was measured for the VisNIR bands M1 and M4 under limited conditions using the NIST T-SIRCUS in post-TVAC testing [1,2]. NASA analysis was reported in [3-5]. This work takes an alternative approach to the analysis based on the calculation of the absolute spectral response (ASR) as described in [6]. Preliminary analysis of the polarization data based on this methodology was reported in [7,8]. The results will then be compared earlier analysis as well as broadband polarization measurements [9]. The test setup and test configuration were reported in earlier works and will not be repeated here.

2. Methodology

The ASR is defined as the ratio of the measured response to the input radiance [6], or

$$ASR(\lambda,\theta) = \frac{dn(\lambda,\theta)}{L(\lambda,\theta)} \tag{1}$$

where λ is the measured wavelength and θ is the polarization angle. As was described in [6], the center wavelength (λ_C), bandwidth (BW), and responsivity (R) can be derived from the ASR as follows

$$\lambda_C(\theta) = \frac{\int d\lambda \lambda ASR(\lambda,\theta)}{\int d\lambda ASR(\lambda,\theta)} \tag{2}$$

$$BW(\theta) = \frac{\int d\lambda ASR(\lambda,\theta)}{\max[ASR(\lambda,\theta)]_\lambda} \tag{3}$$

$$R(\theta) = \int d\lambda ASR(\lambda,\theta) \tag{4}$$

Note that these equations assume a flat spectrum. A corrected ASR can be constructed for different input spectra [6], as defined by

$$ASR'(\lambda,\theta) = ASR(\lambda,\theta)\frac{L_{source}(\lambda)}{L_{source}^{AVG}(\theta)} \tag{5}$$

where

$$L_{source}^{AVG}(\theta) = \frac{\int d\lambda ASR(\lambda,\theta) L_{source}(\lambda)}{\int d\lambda ASR(\lambda,\theta)} \tag{6}$$

The normalization to the average radiance indicates that R will not change with input spectra [6,8].

In earlier analysis, the zeroth and second order Fourier components were written as [3,5]

$$\frac{1}{2}c_0 = \frac{1}{\pi}\int_0^\pi d\theta dn(\lambda,\theta), \tag{7}$$

$$c_2 = \frac{2}{\pi}\int_0^\pi d\theta \cos(2\theta) dn(\lambda,\theta), \tag{8}$$

and

$$d_2 = \frac{2}{\pi}\int_0^\pi d\theta \sin(2\theta) dn(\lambda,\theta). \tag{9}$$

Further, we define the ratios of the second order coefficients to the zeroth order as

$$C_2 = \frac{2c_2}{c_0}, \tag{10}$$

and

$$D_2 = \frac{2d_2}{c_0}. \tag{11}$$

Consider Equation (10) first, substituting in Equation (1), we get

$$C_2(\lambda) = 2\frac{\int_0^{\pi} d\theta L(\lambda,\theta) ASR(\lambda,\theta)\cos(2\theta)}{\int_0^{\pi} d\theta L(\lambda,\theta) ASR(\lambda,\theta)} \tag{12}$$

For this test, the light exiting the integrating sphere is essentially unpolarized; as a result, the radiance exiting the rotating polarizer will not depend on the orientation of the polarizer axis, or

$$L(\lambda,\theta) \to L(\lambda) \tag{13}$$

Therefore Equation (12) becomes

$$\begin{aligned} C_2(\lambda) &= 2\frac{L(\lambda)\int_0^{\pi} d\theta ASR(\lambda,\theta)\cos(2\theta)}{L(\lambda)\int_0^{\pi} d\theta ASR(\lambda,\theta)} \\ &= 2\frac{\int_0^{\pi} d\theta ASR(\lambda,\theta)\cos(2\theta)}{\int_0^{\pi} d\theta ASR(\lambda,\theta)} \end{aligned} \tag{14}$$

To get the band dependent Fourier components, we integrate over the bandpass, or

$$C_2(B) = \frac{\int d\lambda RSR(\lambda) C_2(\lambda)}{\int d\lambda RSR(\lambda)} \tag{15}$$

Noticing that the denominator is just the unpolarized bandwidth (or the average bandwidth over all polarization states) and substituting in Equation (14), gives

$$C_2(B) = \frac{2}{\langle BW(\theta)\rangle_\theta} \int d\lambda RSR(\lambda) \frac{\int_0^{\pi} d\theta ASR(\lambda,\theta)\cos(2\theta)}{\int_0^{\pi} d\theta ASR(\lambda,\theta)} \tag{16}$$

The denominator inside the integral is equivalent to the average ASR over polarization angle multiplied by the interval; as a result, Equation (16) is rewritten as

$$\begin{aligned} C_2(B) &= \frac{2}{\langle BW(\theta)\rangle_\theta} \int d\lambda RSR(\lambda) \frac{\int_0^{\pi} d\theta ASR(\lambda,\theta)\cos(2\theta)}{\pi\langle ASR(\lambda,\theta)\rangle_\theta} \\ &= \frac{2}{\langle BW(\theta)\rangle_\theta} \int d\lambda RSR(\lambda) \frac{\int_0^{\pi} d\theta ASR(\lambda,\theta)\cos(2\theta)}{\pi \max\left[\langle ASR(\lambda,\theta)\rangle_\theta\right]_\lambda RSR(\lambda)} \\ &= \frac{2}{\pi\langle BW(\theta)\rangle_\theta \max\left[\langle ASR(\lambda,\theta)\rangle_\theta\right]_\lambda} \int d\lambda \int_0^{\pi} d\theta ASR(\lambda,\theta)\cos(2\theta) \end{aligned} \tag{17}$$

The order of the integration can be reversed, and the integral rewritten as

$$C_2(B) = \frac{2}{\pi \langle BW(\theta) \rangle_\theta \max\left[\langle ASR(\lambda,\theta) \rangle_\theta\right]_\lambda} \int_0^\pi d\theta \cos(2\theta) \int d\lambda ASR(\lambda,\theta) \tag{17}$$

Now the interior integral is just Equation (4) and the denominator is also equivalent to the responsivity, averaged over polarization angles. Equation (17) then becomes

$$C_2(B) = \frac{2}{\pi \langle R(\theta) \rangle_\theta} \int_0^\pi d\theta \cos(2\theta) R(\theta) \tag{18}$$

The other Fourier component is also reduced in the same manner

$$D_2(B) = \frac{2}{\pi \langle R(\theta) \rangle_\theta} \int_0^\pi d\theta \sin(2\theta) R(\theta) \tag{19}$$

The degree of linear polarization (DoLP) is then written as

$$\begin{aligned} DoLP(B) &= \left[C_2^2 + D_2^2\right]^{1/2} \\ &= \frac{2}{\pi \langle R(\theta) \rangle_\theta} \left[\int_0^\pi d\theta_1 \cos(2\theta_1) R(\theta_1) \int_0^\pi d\theta_2 \cos(2\theta_2) R(\theta_2) + \int_0^\pi d\theta_1 \sin(2\theta_1) R(\theta_1) \int_0^\pi d\theta_2 \sin(2\theta_2) R(\theta_2)\right]^{1/2} \\ &= \frac{2}{\pi \langle R(\theta) \rangle_\theta} \left[\int_0^\pi d\theta_1 R(\theta_1) \int_0^\pi d\theta_2 R(\theta_2) \left[\cos(2\theta_1)\cos(2\theta_2) + \sin(2\theta_1)\sin(2\theta_2)\right]\right]^{1/2} \\ &= \frac{2}{\pi \langle R(\theta) \rangle_\theta} \left[\int_0^\pi d\theta_1 R(\theta_1) \int_0^\pi d\theta_2 R(\theta_2) \cos(2\theta_1 - 2\theta_2)\right]^{1/2} \end{aligned} \tag{20}$$

and the phase angle is now written as

$$\begin{aligned} Phase(B) &= \tan^{-1}\left[\frac{D_2}{C_2}\right] \\ &= \tan^{-1}\left[\frac{\int_0^\pi d\theta \sin(2\theta) R(\theta)}{\int_0^\pi d\theta \cos(2\theta) R(\theta)}\right] \end{aligned} \tag{21}$$

Here no polarizer efficiency correction was used in the DoLP, but for this test the effect was minor.

Note that the responsivity is the product of the maximum ASR over wavelength and the bandwidth. As was observed previously, the shifting in the edges of the bandpass was causing the large DoLP and here the DoLP is now an explicit function of the change in bandwidth with polarization angle.

3. Analysis and Results

First, the ASR was constructed for each polarization angle and wavelength. The processing of the dn was described in [5]. Radiance information on the source during the polarization testing was available; however, the radiance data was collected before the light had passed through the rotating polarizer. To determine the transmission factor for the BVONIR polarizer, the unpolarized ASR was compared to the ASR constructed from earlier spectral testing using the T-SIRCUS [10]. The average transmission was estimated for each band, HAM side, and scan angle. This transmission factor was then applied to the polarized ASR. As noted in earlier work [3,5], some data did not meet the quality control criteria; these missing polarizer angles for some wavelengths were reconstructed from the analysis in [3,5]. Examples of the ASR for bands M1 (top) and M4 (bottom) are shown in Figure 1 for detector 9, scan angle -8, HAM side 1 data. The different curves represent the ASR for the 13 measured polarization angles (plus the unpolarized ASR). Note that although the spectral bands were under-sampled, the general shape of the bandpass is well described [10]. As a measure of repeatability, 0 and 180 degrees polarization angles were treated separately; the two measurements generally agreed to within 1 %, but could disagree by up to 3 % in the lowest response points. There is some variability between the different polarization states on the sides of the M1 and M4 bandpasses and also in the structure of the center of the M4 bandpass. These features are largely responsible for the higher than expected band average polarization sensitivity observed in broadband testing [4]. The ASR constructed for the remaining detectors and measurements show similar variability, although there is a fair amount of detector dependence.

The variations observed in the center of the bandpass for M4 correspond to a spectral region where a phase shift occurs [3]. Analysis has shown that a similar phase shift pattern occurs in the same spectral region for Day Night Band (DNB) data [11], indicating that this phenomena is not caused by the spectral band filters. Ray trace modeling conducted by Raytheon did not predict this behavior [4]; the root cause of this behavior is under investigation.

The calculated band M1 centroids and bandwidths derived from the flat spectrum ASR functions are shown in Figures 2(a) and (c); similarly, the M4 centroids and bandwidths are shown in Figures 2(b) and (d). Although Figure 2 only shows results from measurements made at -8 degrees scan angle, HAM side 1, the results shown are indicative of all the test configurations measured. Note that the centroids and bandwidths derived from unpolarized data are plotted as the disconnected points at 195 degrees. The variation in centroid is small, up to ~ 0.2 nm for M1 and ~ 0.3 nm for M4. The bandwidth, however, varies by up to ~ 1.5 nm for M1 and ~ 1.7 nm for M4. There is also significant detector-to-detector dependence in M4 for the bandwidth, with the smallest variation being as low as ~ 0.5 nm. The broadening or narrowing of the bandpass with polarization state leads to greater polarization sensitivity on the band edges and, as a result, larger band average polarization sensitivity. The average centroids determined from spectral testing [10] were 411.8 nm and 556.9 nm for M1 and M4, respectively; the M1 and M4 values are both slightly lower than spectral testing. The band average bandwidths derived from spectral testing were 18.2 nm (M1) and 18.1 nm (M4); the M1 values are slightly lower here while the M4 bandwidths are slightly higher. Note that this may be the result of the spectral bandpass in this testing being under-sampled.

The responsivity for M1 derived using -8 degrees scan angle, HAM side 1 data is shown in Figure 3(a) as a function of polarization angle. Similar responsivity graphs for M1 derived using +45 degrees scan angle, HAM side 1 data [Figure 3(b)], M4 derived using -8 degrees scan angle, HAM side 1 data [Figure 3(c)], and M4 derived using +45 degrees scan angle, HAM side 1 data [Figure 3(d)] are also shown. The responsivities for M4 derived using -8 degrees scan angle, HAM side 0 data are not shown, but are consistent with Figures 3(c) and (d). In addition, the responsivity derived from unpolarized data is shown as the unconnected data at 195 degrees in each sub-figure. The responsivities vary by up to ~ 6.9 % for M1 and ~ 4.5 % for M4, relative to the average value over polarization angles. Again, there is some detector dependence for M1 (the responsivities vary by between ~ 4.5 and ~ 6.9 % at -8 degrees scan angle and between ~ 6.3 and ~ 6.9 % at +45 degrees scan angle) and higher detector dependence for M4 (the responsivities vary by between ~ 0.8 and ~ 4.5 % at -8 degrees scan angle and between ~ 1.4 and ~ 4.1 % at +45 degrees scan angle). The observed detector dependence is consistent with broadband polarization measurements [4]. The band average responsivities derived from separate unpolarized radiometric measurements [12] are 18.2 (M1) and 34.1 (M4), which are slightly lower than the unpolarized values reported here. This small discrepancy may result from the under-sampling for the spectral bandpass.

Examples of the unpolarized ASR convolved with the SIS and TOA spectra are shown in Figure 4 for both M1 (a) and M4 (b) using data from detector 9, -8 degrees scan angle, HAM side 1. The SIS spectra is fairly smooth and increasing in these spectral regions from blue to red, while the TOA spectra decreases from blue to red and includes some structure. This causes the SIS spectra to shift the ASR curve to longer wavelengths and the TOA spectra to shift the ASR curve to shorter wavelengths. The structure in the TOA spectra is the source of the slight downturn in the ASR curve observed in the middle of the M1 bandpass.

The centroids derived from -8 degrees scan angle, HAM side 1 data are graphed in Figure 5 for M1 convolved with the SIS (a) and TOA (b) spectra and for M4 convolved with the SIS (c) and TOA (d) spectra. The maximum variability with polarization state is about the same across the different input spectra and also when compared to the centroids derived from the flat spectra, shown in Figures 2(a) and (b). The band average M1 centroid determined from the unpolarized ASR function increased by ~ 0.65 nm from flat to SIS spectra and decreased from flat to TOA spectra by about 0.2 nm. In the case of M4, the corresponding changes were ~ 0.2 and ~ −0.3 nm.

Figure 6 shows the bandwidths as a function of polarization state derived from the M1 ASR curves convolved with the SIS (a) and TOA (b) spectra as well as the M4 ASR curves convolved with the SIS (c) and TOA (d) spectra (using data collected at -8 degrees scan angle, HAM side 1). The band average unpolarized bandwidths are ~ 1.4 nm (M1) and ~ 0.3 nm (M4) lower when the ASR functions are convolved with the SIS spectrum and ~ 0.2 nm higher (M1) and ~ 0.1 nm lower (M4) when the ASR functions are convolved with the TOA spectrum. In addition, the variability over polarization state differs from the flat input spectrum: the maximum bandwidth changes with polarization state are ~ 0.9 and ~ 1.5 nm for M1 using the SIS and TOA spectra respectively and ~ 2.1 and ~ 0.9 nm for M4 using the SIS and TOA spectra respectively. The bandwidth as calculated from Eq. (3) will vary between different input spectra solely due to changes in maximum ASR over wavelength [the responsivity is invariant under the convolution as defined in Eq. (5)]. Changes in the maximum ASR value across polarization state leads to the bandwidth estimates deviating from a clean two cycle oscillation as seen in Figures 6(a) and (d). This is believed to result largely from the under-sampling of the bandpass during T-SIRCUS testing. Furthermore, the bandwidths derived from unpolarized data should be roughly equivalent to the average over all the bandwidths derived from polarized data; however, as seen in Figures 6(a) and (d), this is not always the case.

The comparison of the DoLP between Eq. (20) and [3] is shown in Figure 7. The left plots show all measured cases using the baseline approach (black) and the current approach (red) while the right plots show the difference between the two sets of results. For the M1 measurements, the differences are below 0.15 % while the M4 measurements agree to with a difference of 0.1 %. The phase differences are shown in Figure 8 using the same format. The phase angles generally agree well for the low number detectors and the differences increase with detector number, to as high as 4 degrees in M1 and 6 degrees in M4. Note that some small amount of missing data was reconstructed using the analysis in [3], which may account for some of the differences.

7. Summary

T-SIRCUS polarization testing was performed under ambient conditions, post-TVAC for the JPSS-1

VIIRS sensor. Re-analysis in terms of the ASR has shown the following:

- The DoLP and phase angle can be derived from the ASR formulation. Both of these reduce to functions of the responsivity with polarization angle. As the responsivity is just the product of the maximum ASR over wavelength and the bandwidth, the DoLP and phase angle are explicitly dependent on the bandwidth. Ray-trace model had shown that it was variations in bandpass with polarization angle that were driving the polarization sensitivity.
- Derived centroids and bandwidths are slightly lower than earlier testing for both M1 and M4, likely due to under-sampling. Responsivities are also slightly lower than those derived in earlier testing.
- The ASR was convolved with SIS and TOA spectra. Changes tended to be small, with centroid changes below ~0.65 nm and bandwidth changes below 1.4 nm.

Figure 1: Plots are shown of the ASR measured for M1 (upper plot) and M4 (lower plot). All data shown was collected at detector 9, -8 degrees scan angle, HAM side 1.

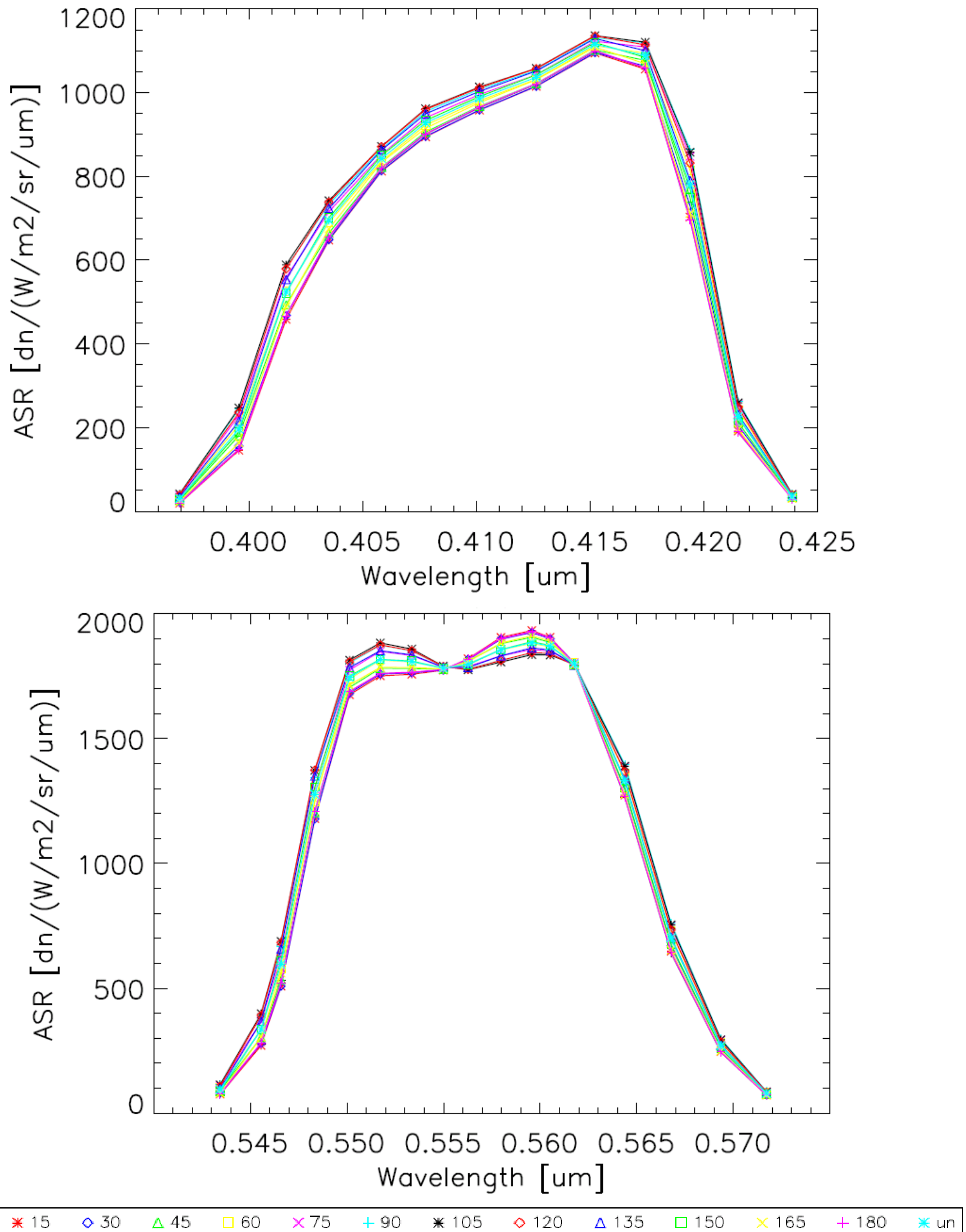

Figure 2: Plots are shown of the band centroid for M1 (a), the band centroid for M4 (b), the bandwidth for M1 (c), and the bandwidth for M4 (d) versus polarization state. All data shown was collected at -8 degrees scan angle, HAM side 1.

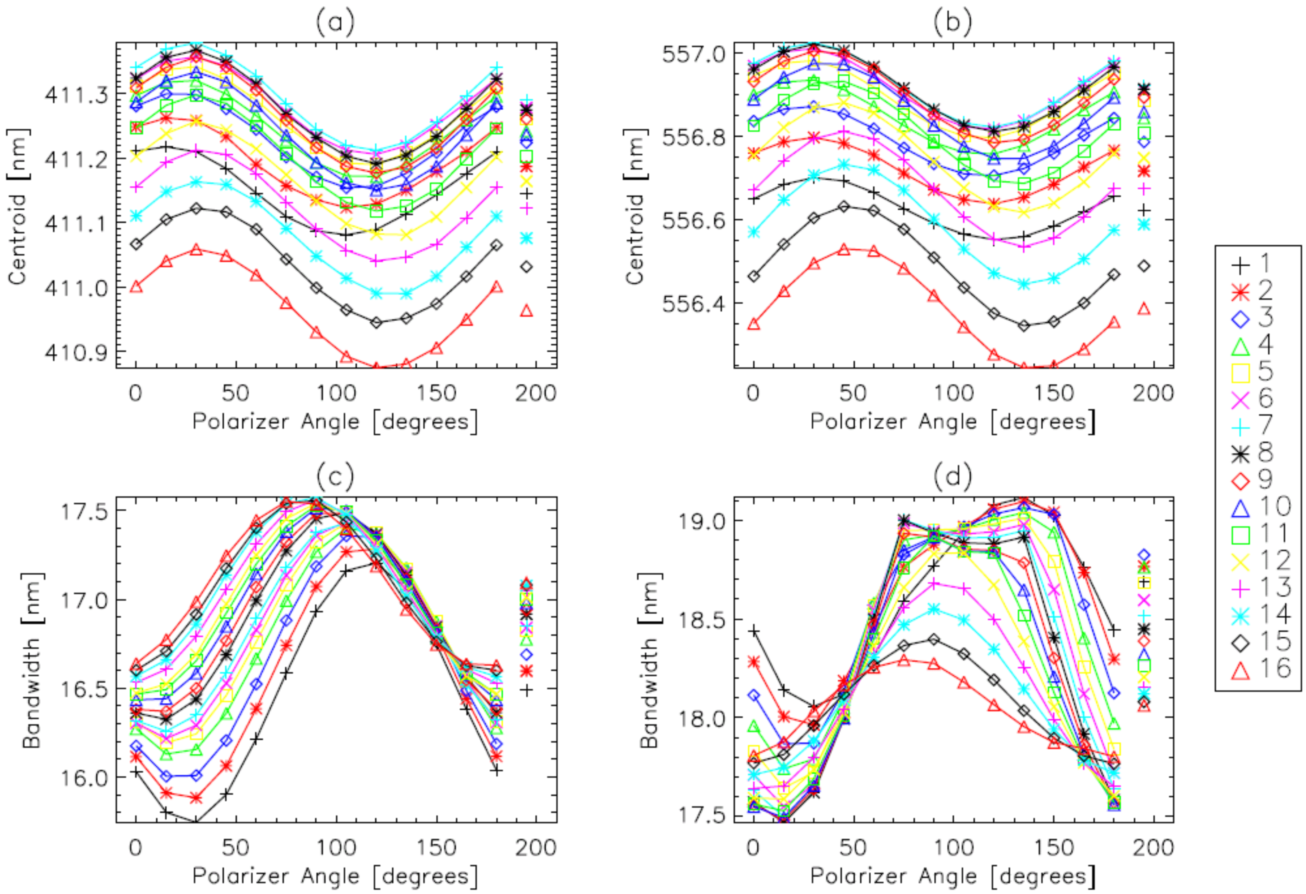

Figure 3. Plots are shown of the responsivity versus polarization state for M1 at -8 degrees scan angle (a), for M1 at +45 degrees scan angle (b), for M4 at -8 degrees scan angle (c), and for M4 at +45 degrees scan angle (d). All data shown was collected using HAM side 1 and the responsivity is in units of [dn/(W/m2/sr/μm)].

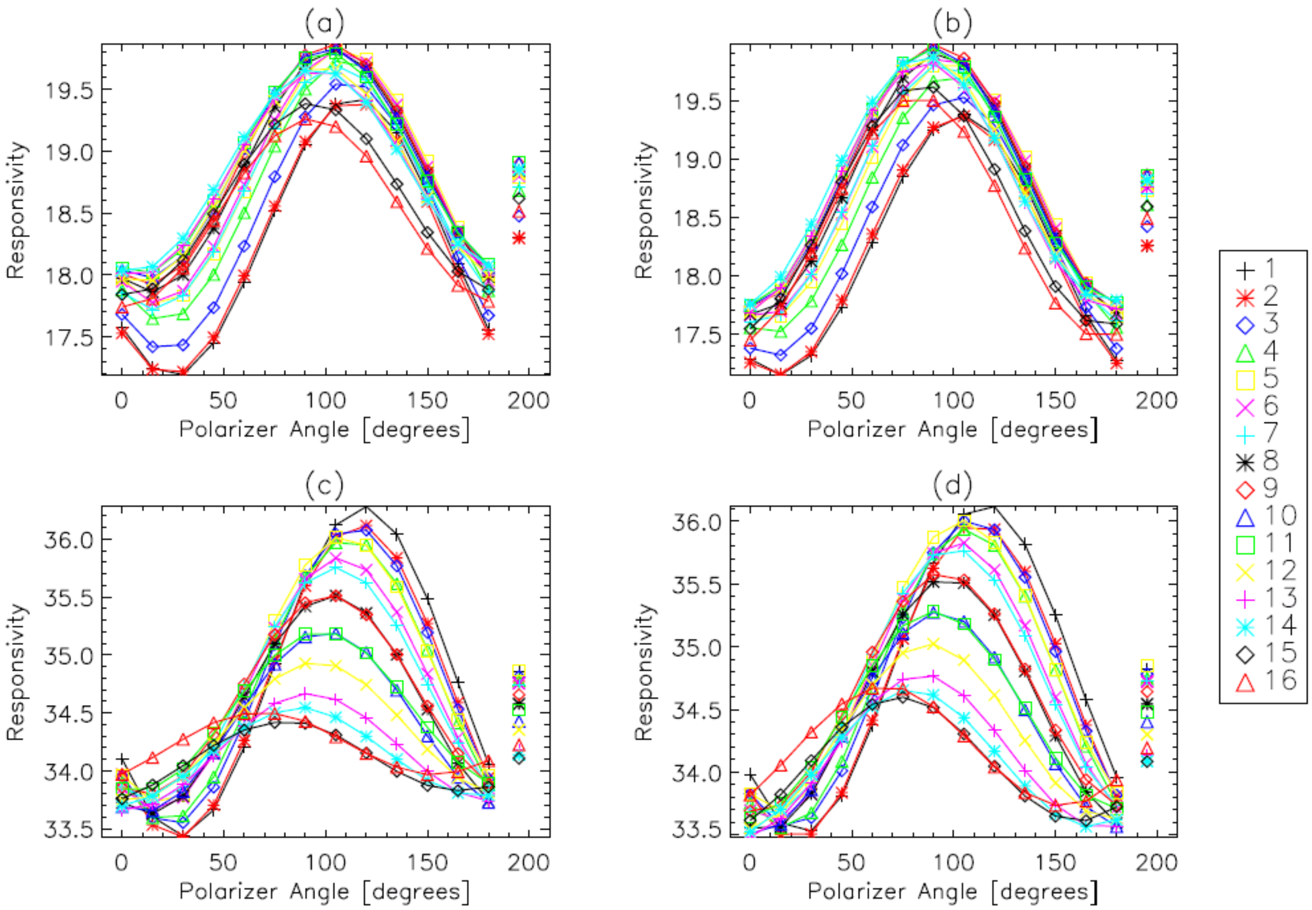

Figure 4. M1 ASR shown for detector 9 using data collected at -8 degrees scan angle, HAM side 1 (a) and M4 ASR shown for detector 9 using data collected at -8 degrees scan angle, HAM side 1 (b).

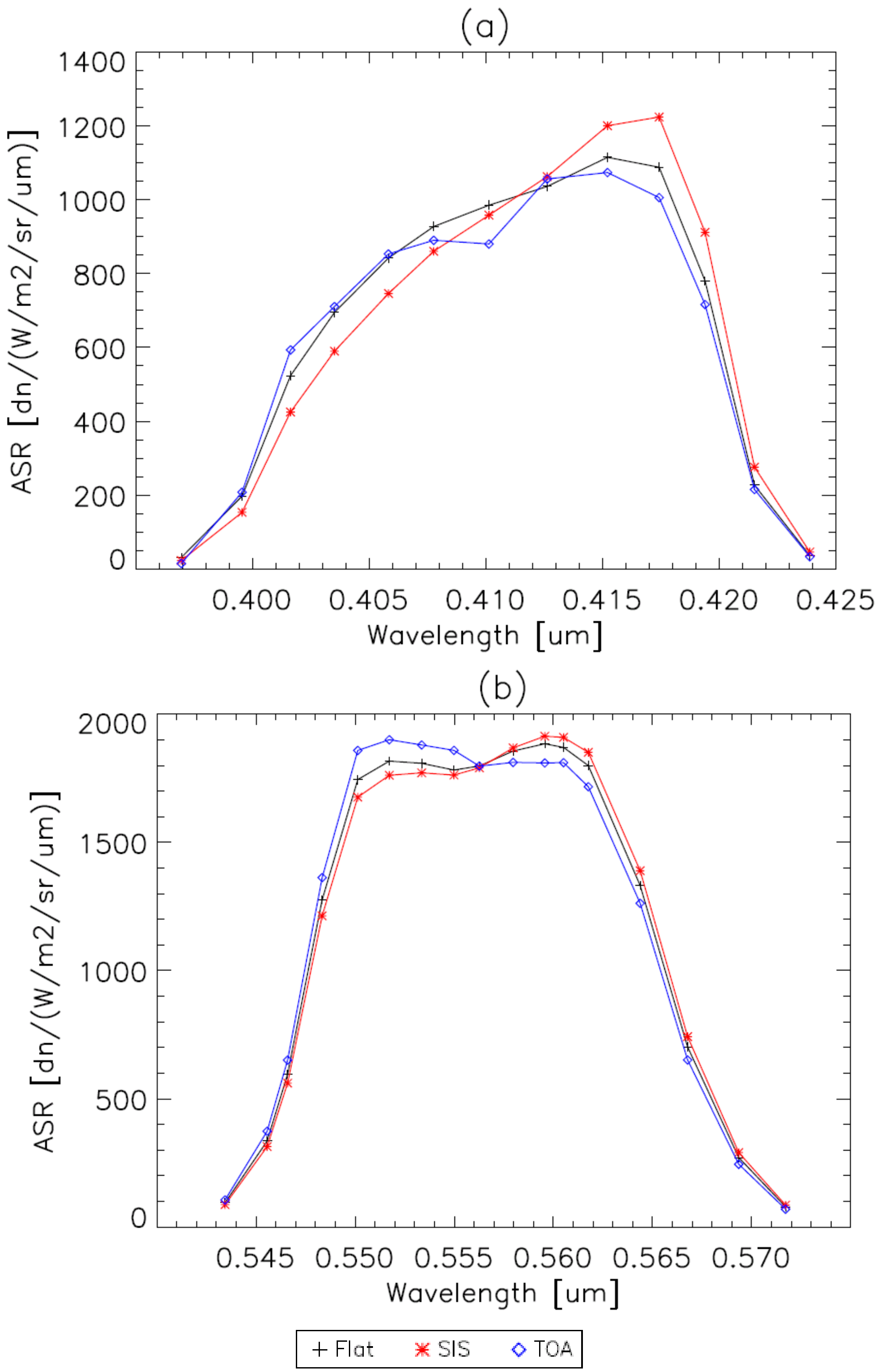

Figure 5. Plots of the band centroid versus polarization state for M1 using the SIS spectrum (a), M1 using the TOA spectrum (b), M4 using the SIS spectrum (c), and M4 using the TOA spectrum (d). All data shown is from -8 degrees scan angle, HAM side 1.

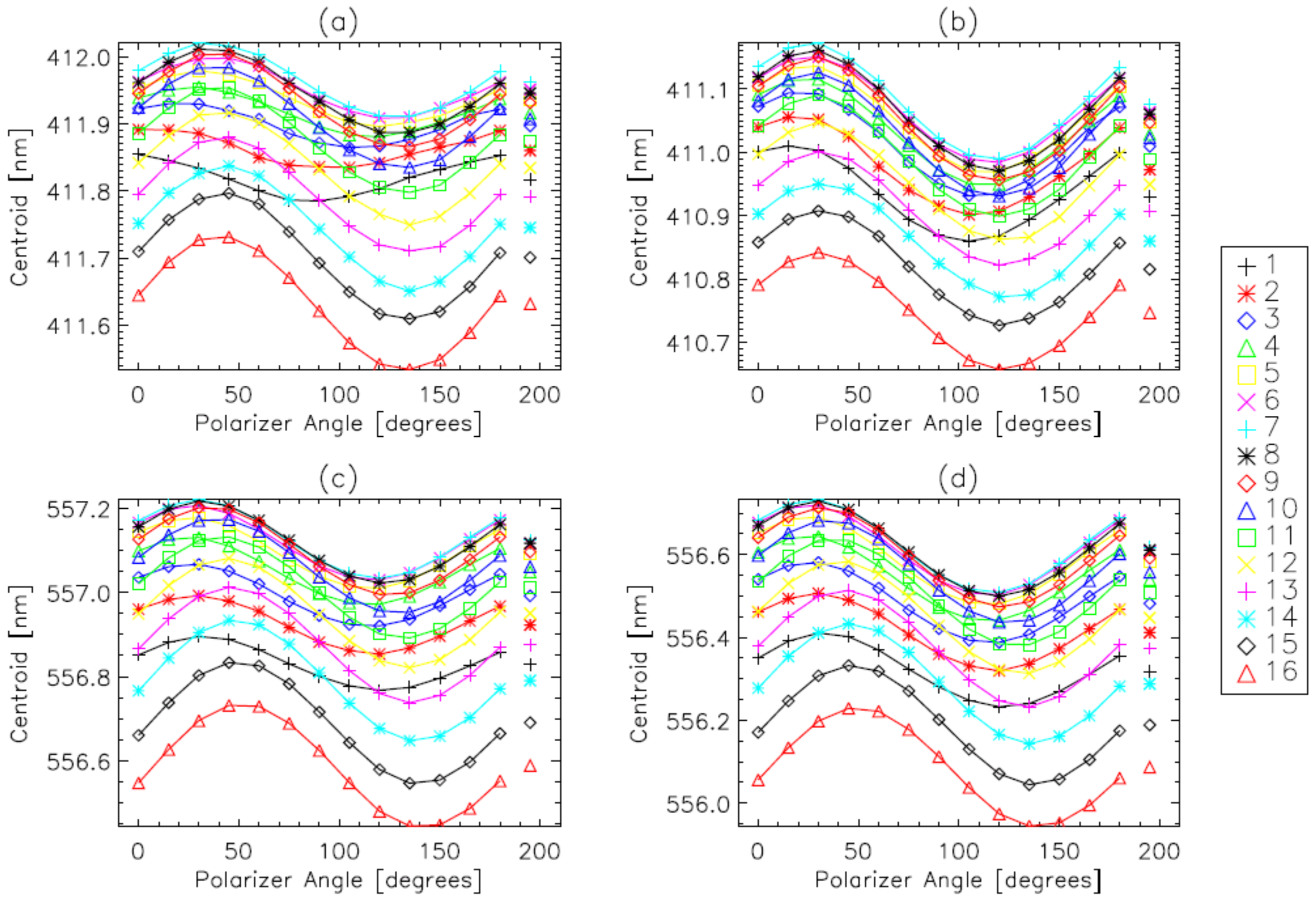

Figure 6. Plots of the bandwidth versus polarization state for M1 using the SIS spectrum (a), M1 using the TOA spectrum (b), M4 using the SIS spectrum (c), and M4 using the TOA spectrum (d). All data shown is from -8 degrees scan angle, HAM side 1.

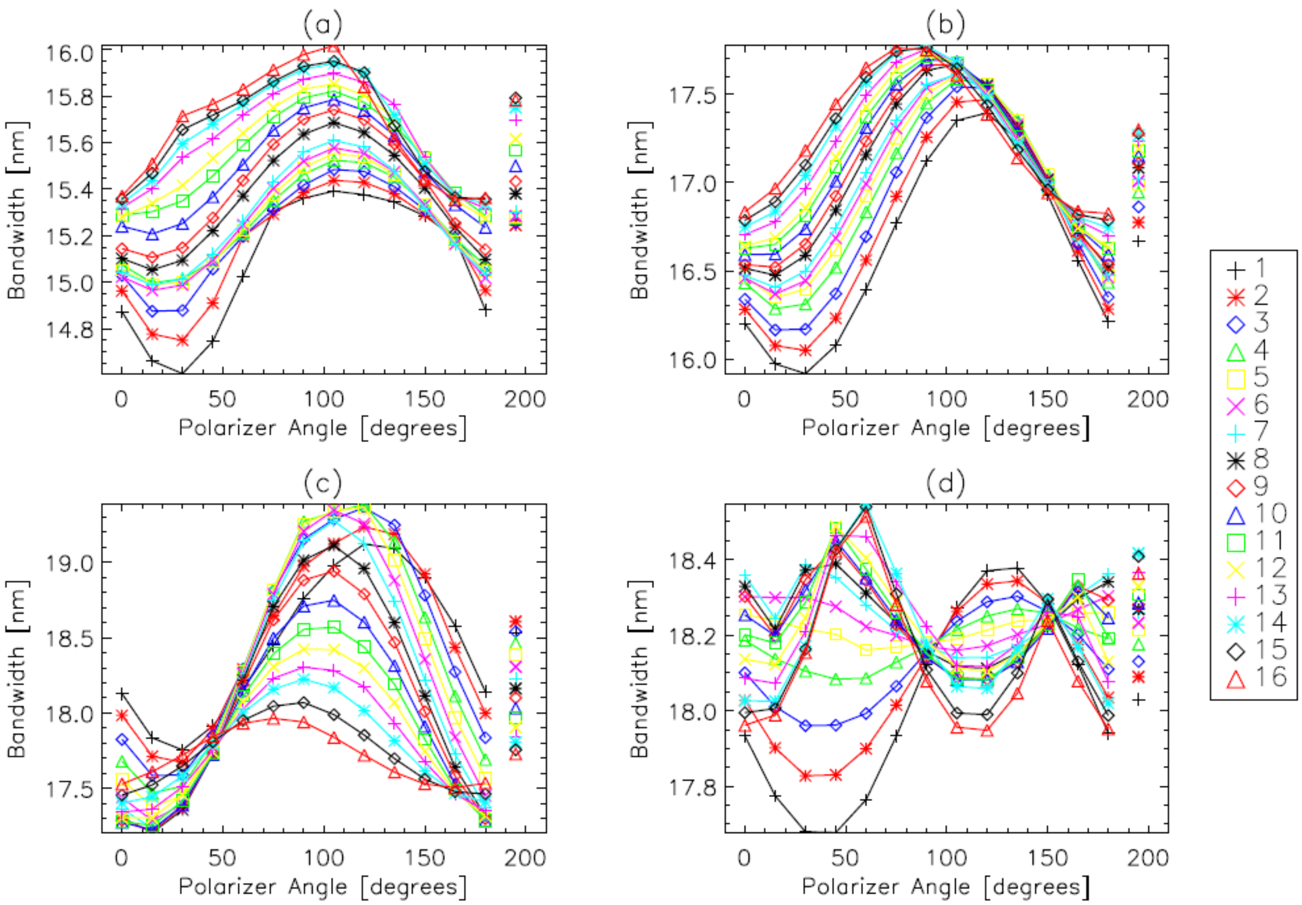

Figure 7: Comparison of DoLP results from the present methodology and that presented in [3]. The comparison is plotted on the left and the difference between the two approaches is plotted on the right.

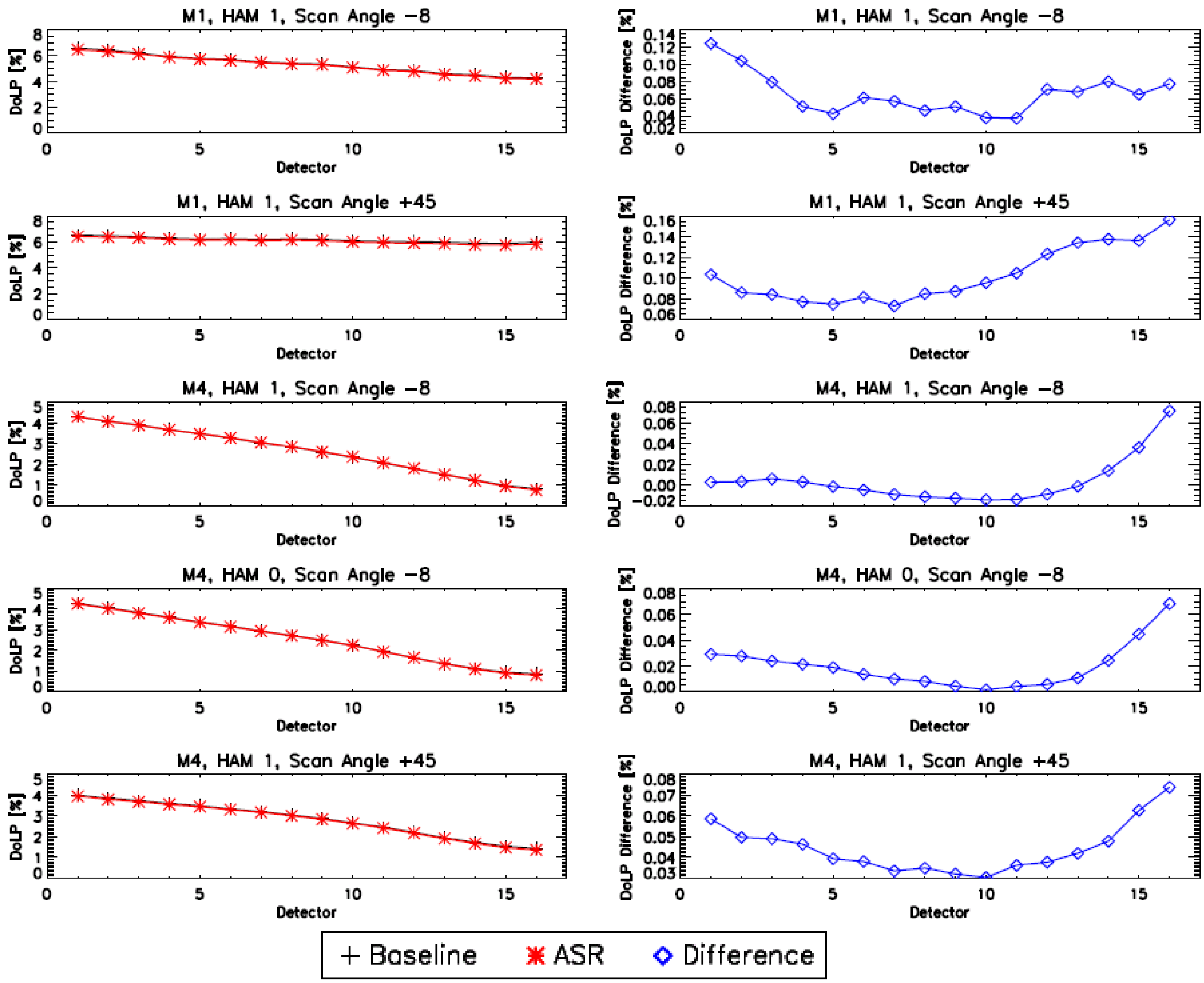

Figure 8: Comparison of phase angle results from the present methodology and that presented in [3]. The comparison is plotted on the left and the difference between the two approaches is plotted on the right.